Multidimensional laser cooling of broad- and narrow-line $0 \leftrightarrow 1$ dipole transitions

Daniel J. Phalen, Colin C. Young,* Su Yi, and Han Pu
Department of Physics and Astronomy, and Rice Quantum Institute, Rice University, Houston, Texas 77251-1892, USA
(Received 12 November 2004; revised manuscript received 23 May 2005; published 14 September 2005)

We present a detailed study of laser cooling of neutral atoms with an electric-dipole transition between a $J_g=0$ ground state and a $J_e=1$ excited state, for both broad- and narrow-line transitions. We focus on the novel effects arising from the multidimensional nature of the laser configuration and point out under which conditions these features can be observed in practice. Our analysis also shows that qualitative differences in multidimensional laser cooling properties exist between the broad- and the narrow-line transitions.

DOI: 10.1103/PhysRevA.72.033406 PACS number(s): 32.80.Pj, 32.80.Lg, 39.25.+k, 42.50.Vk

I. INTRODUCTION

Cooling and trapping of neutral atoms has matured over the past two decades or so, and ultracold atomic physics is now one of the most active areas of physics. Various laser cooling mechanisms have been identified, among which the two most important ones are the Doppler and Sisyphus cooling mechanisms. Although many experiments are performed with three-dimensional (3D) laser configurations, theoretical efforts in cooling and trapping have disproportionally concentrated on 1D optical fields [1] with the implicit assumption that light-pressure forces in higher dimensions would just be a simple superposition of 1D forces. This, however, has been shown not to be true in general—there are inherently multidimensional effects that cannot be accounted for by a 1D theory [2–5] and that may play important roles for the atomic kinematics and dynamics in optical molasses and magneto-optical traps (MOT's). Evidence of multidimensional effects was found in the experiment of Ref. [6] where two near-resonant laser standing waves along orthogonal directions were used.

In the current paper, we want to examine in detail the multidimensional laser cooling features for an atom possessing an electric-dipole transition between a $J_g=0$ ground state and a $J_e=1$ excited state and subject to a 2D σ^+-σ^- laser field. We pick this particular system for several important reasons. First, this system is often used as a paradigm to illustrate the mechanism of the MOT [7], which has become a standard tool in most laser cooling and trapping laboratories. It has been assumed that the 1D MOT mechanism could be straightforwardly generalized to 3D by applying σ^+-σ^- light fields along three mutually orthogonal directions, thus excluding any potential multidimensional effects. It is therefore important to investigate whether this assumption is valid.

Second, our work is motivated by the recent experimental efforts on cooling and trapping of alkaline-earth atoms, such as calcium [8] and strontium [9–11]. Due to the lack of hyperfine structure, the bosonic alkaline-earth atoms possess singlet ground states ($J_g=0$) and several triplet $J_e=1$ excited states. The simple level structure makes these atoms ideally suited for optical-frequency standard and cold collision studies [12]. Some of the triplet excited states have linewidths comparable to or even narrower than the single-photon recoil frequency, which offers the possibility of cooling the atom down below the single-photon-recoil limit using Doppler cooling. A recent experiment done at JILA [13] on ^{88}Sr indeed demonstrated this possibility with red-detuned σ^+-σ^- light fields. The same experiment also showed the formation of momentum-space lattice structure when the laser detuning is changed to the blue side. This experiment is carried out with a 3D laser field, but it seems that the results can be explained by a simple 1D theory [13]. In addition to the alkaline-earth atoms, the rare-earth atom Yb also possesses a similar ground-state structure. Recently, a condensate of Yb atoms has been achieved with the help of the narrow-line cooling [14].

In this paper, we will provide a detailed investigation of the light-pressure force and momentum-space distribution for an atom with a $J_g=0 \leftrightarrow J_e=1$ dipole transition in a 2D $\sigma^+\sigma^-$ laser field, focusing on the multidimensional effects and the differences between the broad- and narrow-line transitions. We will also comment on why the multidimensional features are absent in the JILA experiment and find conditions under which these features will manifest themselves. After discussing our model in Sec. II, we will present in Secs. III and IV the results for the broad- and narrow-line transitions, respectively. Concluding remarks are presented in Sec. V. In Appendix A, we will present an analytical approach to calculate the light-pressure forces for the broad-line transition. Finally, in Appendix B, We will examine the effects of a uniform external magnetic field.

II. MODEL

We choose the quantization axis to be along the z axis. As shown in Fig. 1, the ground state is denoted by $|g\rangle$ and the three Zeeman sublevels of the excited manifold are denoted by $|+\rangle$, $|0\rangle$, and $|-\rangle$, which are coupled to the ground state with light polarized along $\hat{\sigma}^+$, $\hat{z}$, and $\hat{\sigma}^-$, respectively, where

$$\hat{\sigma}^{\pm} = (\mp \hat{x} - i\hat{y})/\sqrt{2} \tag{1}$$

are spherical unit vectors with respect to the quantization axis z.

*Present address: Dept. of Physics, Tulane University, New Orleans, LA 70118, USA.

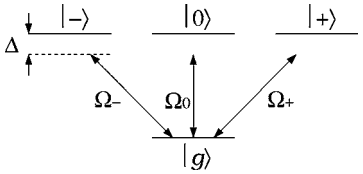

FIG. 1. Level scheme of the $J_g=0\leftrightarrow J_e=1$ dipole transition.

For the 2D laser configuration considered in this work, we choose the laser fields to be propagating along the $\pm x$ and $\pm y$ directions and polarized along $\hat{\sigma}_x^{\pm}$ and $\hat{\sigma}_y^{\pm}$, respectively, where $\hat{\sigma}_{x,y}^{\pm}$ can be obtained from $\hat{\sigma}^{\pm}$ in Eq. (1) by cyclically permuting $(\hat{x},\hat{y},\hat{z})$. The electric field can then be written as

$$\mathbf{E}=\frac{1}{2}[E_x(\hat{\sigma}_x^{+}e^{ikx}+\hat{\sigma}_x^{-}e^{-ikx})+e^{i\phi}E_y(\hat{\sigma}_y^{+}e^{iky}+\hat{\sigma}_y^{-}e^{-iky})]e^{-i\omega t}+\text{c.c.},$$

where ϕ denotes the time-phase difference between the fields along the two orthogonal directions and can be restricted between 0 and π. Previous studies have shown that this phase may significantly affect the 2D light-pressure force [4–6]. We can rewrite the electric field, or equivalently the Rabi frequency, under the polarization vector basis $(\hat{\sigma}^{+},\hat{\sigma}^{-},\hat{z})$, as

$$\Omega_{\pm}=\Omega_x\sin kx\pm ie^{i\phi}\Omega_y\cos ky, \tag{2a}$$

$$\Omega_0=-i\sqrt{2}\Omega_x\cos kx-i\sqrt{2}e^{i\phi}\Omega_y\sin ky, \tag{2b}$$

where $\Omega_{x,y}=dE_{x,y}/(2\hbar)$, with d being the transition dipole moment, which can be assumed to be real without loss of generality.

The Hamiltonian under the rotating-wave approximation describing the dipole coupling reads

$$H=\frac{1}{2m}(P_x^2+P_y^2)-\hbar\Delta(\rho_{--}+\rho_{00}+\rho_{++})-\frac{\hbar}{2}(\Omega_-\rho_{-g}+\Omega_0\rho_{0g}+\Omega_+\rho_{+g}+\text{H.c.}), \tag{3}$$

where $\rho_{ij}=|i\rangle\langle j|$ $(i,j=g,-,0,+)$ and Δ is the detuning of the laser fields from the atomic transition. In writing the Hamiltonian, we have neglected the kinetic energy $P_z^2/(2m)$, and since the laser fields are applied only along the x and y axes, the atomic center-of-mass motion along the z axis is neglected.

In the following, we will present our results for the broad- and narrow-line transitions separately.

III. RESULTS FOR THE BROAD-LINE TRANSITION

For the broad-line transition, the momentum width of the atom is much larger than the single-photon recoil momentum. Under this condition, the atom can be regarded as a point particle and the standard semiclassical approach can be used, in which the center-of-mass motion of the atom is not quantized and the atomic velocity comes into the picture as a c-number parameter.

A general 2D semiclassical theory can be found in Ref. [5], where a numerical technique based on the continued-fraction method for calculating the velocity-dependent light-pressure force was presented. This theory is, in principle, valid for arbitrary electric-dipole transitions and arbitrary 2D laser configurations. For the $J_g=0\leftrightarrow J_e=1$ transition we are interested in here, the relatively simple level structure also allows us to present an analytical calculation under the weak-field low-velocity limit that is valid for arbitrary dimensions, which can provide significant insights into the multidimensional nature of the system. Both of these approaches will be used here to calculated the velocity-dependent forces.

To find the velocity-dependent force, we first obtain the steady-state solutions of the optical Bloch equations:

$$\dot{\rho}_{ij}=\mathbf{v}\cdot\boldsymbol{\nabla}\rho_{ij}=\frac{1}{i\hbar}[\rho_{ij},H]+\mathcal{L}[\rho_{ij}],$$

where $\mathbf{v}$ is the velocity of the atom and $\mathcal{L}[\rho_{ij}]$ represents the phenomenological damping terms. The light-pressure force is then found by substituting the steady-state solutions of ρ_{ij}'s into the formula

$$\mathbf{F}(\mathbf{v})=-\overline{\langle\boldsymbol{\nabla}H\rangle},$$

where the overbar denotes a spatial average over the laser wavelength.

A. 1D results

It is instructive to first briefly mention the situation where only a 1D σ^{+}-σ^{-} laser field is applied. For this case, it is convenient to choose the propagation direction along the $\pm z$ axis. Assuming the two fields have equal intensity, we then have $\Omega_0=0$ and $\Omega_{\pm}=\Omega e^{\pm ikz}$, where Ω is a constant and can be taken to be real, and k is the wave number of the fields. Under such a field configuration, the $J_g=0\leftrightarrow J_e=1$ transition reduces to a three-level V system since the $|0\rangle$ excited sublevel is not coupled to the ground state. The conservation of angular momentum prevents a coherent photon redistribution (i.e., the atom absorbs a photon from one field followed by a stimulated emission into the other field) from occurring. Consequently, in this 1D situation, the light-pressure force consists entirely of the spontaneous force [15] which is a superposition of the radiation pressure exerted by the two individual running light fields. The force can be readily found analytically as

$$F(v_z)=\hbar k\beta\left[\frac{s}{1+s+(\Delta-kv_z)^2/\beta^2}-\frac{s}{1+s+(\Delta+kv_z)^2/\beta^2}\right], \tag{4}$$

where 2β is the excited-state spontaneous decay rate and $s=\Omega^2/(2\beta^2)$ is the saturation parameter (the ratio of the single-beam laser intensity and the saturation intensity).

By examining the expressions of the Rabi frequencies in Eqs. (2), we can immediately see one major difference between the 2D and 1D field configurations: while in the latter case the field is composed of running waves with orthogonal polarizations, in the former case the waves traveling along different directions possess parallel polarization components. Consequently, the field in the 2D case contains standing-wave patterns, as manifested by the sinusoidal functions in

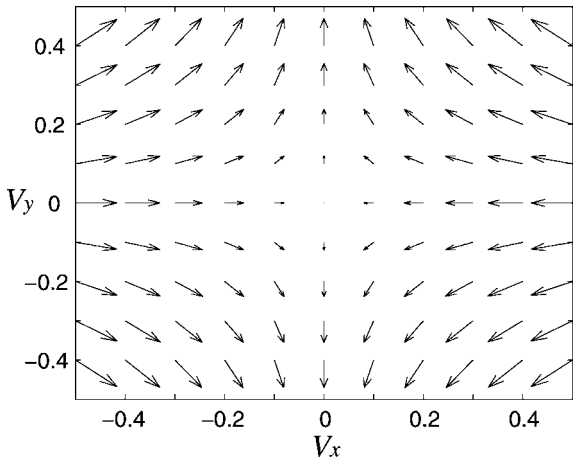

FIG. 2. Velocity-dependent force for $\Delta=0$, $s=5$, and $\phi=\pi/4$. The velocity is in units of β/k.

the expressions of Rabi frequencies [see Eqs. (2)], which makes a coherent photon redistribution possible. Therefore in the 2D situation the light-pressure force should have a stimulated component that is completely absent in the 1D case.

We now turn to our 2D results.

B. 2D results

With the 2D laser field, in general, we have to resort to numerical calculations to solve the optical Bloch equations. However, the simple level structure we consider here also affords an analytical expressions of the light pressure under the weak intensity low-velocity limit. The details of the numerical technique we use can be found in Ref. [5]. Here we only present the results from this calculation. In the examples shown, we always take $\Omega_x=\Omega_y=\Omega$ and $s=\Omega^2/(2\beta^2)$. We will discuss the cases for weak and strong light field intensities separately.

1. Weak-intensity limit

Figure 2 shows a vector plot of the velocity-dependent force as a function of (v_x,v_y). Here the laser is on-resonance $(\Delta=0)$, the phase $\phi=\pi/4$, and the saturation parameter $s=5$. In this case, the force is strongly anisotropic—it is a cooling force along the x axis, while a heating force along the y axis. Similar behavior was found for a two-level atom in a 2D laser field [4,6]. It can be understood from the pattern of the Poynting vector of the field and can be identified as a spontaneous force. As in the case of the two-level atom, this anisotropic force is sensitive to the time-phase difference ϕ. Numerically, we found that it varies as $\sin 2\phi$; hence it vanishes for $\phi=0$ and $\pi/2$, changes sign when $\phi\rightarrow\phi+\pi/2$.

To gain more insights into the results shown in Fig. 2, we solve the optical Bloch equations analytically in the weak-field limit, i.e.,

$$\Omega^2 \ll \beta^2+\Delta^2,$$

by generalizing the procedures outlined in Ref. [16] for a two-level atom. The details can be found in Appendix A. This analytic calculation is valid for arbitrary dimensions. With the 2D σ^+-σ^- field configuration, to first order in atomic velocity, we find that the force can be decomposed into an isotropic and an anisotropic part $\mathbf{F}(\mathbf{v})=\mathbf{F}_{\rm iso}(\mathbf{v})+\mathbf{F}_{\rm ani}(\mathbf{v})$ with

$$\mathbf{F}_{\rm iso}(\mathbf{v}) = \alpha_{\rm iso}\hbar k^2(v_x\hat{x}+v_y\hat{y}), \tag{5a}$$

$$\mathbf{F}_{\rm ani}(\mathbf{v}) = \alpha_{\rm ani}\hbar k^2(v_x\hat{x}-v_y\hat{y}), \tag{5b}$$

where the dimensionless coefficient for the anisotropic force is given by

$$\alpha_{\rm ani} = \frac{3(\Delta^2-3\beta^2)\Omega^4}{32(\beta^2+\Delta^2)^3}\sin 2\phi, \tag{6}$$

in agreement with the numerical results. The corresponding isotropic force coefficient has the following expression:

$$\alpha_{\rm iso} = \alpha_{\rm 1D} - \frac{\Delta\Omega^4}{32\beta(\beta^2+\Delta^2)^3} \times[122\beta^2-8\Delta^2-3(5\beta^2+\Delta^2)\cos 2\phi], \tag{7}$$

where $\alpha_{\rm 1D}=2\Delta\beta\Omega^2/(\beta^2+\Delta^2)^2$ is the coefficient for the 1D force which can be easily obtained from Eq. (4). The isotropic force therefore vanishes at $\Delta=0$ (see Fig. 2). In the weak-field limit when this analytic treatment is valid, the isotropic force will in general dominate over the anisotropic force for finite detunings as $\alpha_{\rm 1D}$ is the most dominant component of the force coefficients.

2. Strong-intensity limit

Figure 3 shows three examples of the velocity-dependent force for a strong field. Here the laser is red-detuned $(\Delta<0)$; hence, according to the 1D theory [Eq. (4)], we should expect a cooling force. The bottom plot of Fig. 3, with $\phi=\pi/2$, does show a cooling force in the entire velocity space. By contrast, in the case when $\phi=0$ and $\pi/4$ (upper and middle plots of Fig. 3), we see a cooling force at large atomic velocities, but a heating force as the velocity decreases below some critical value. For $\phi=\pi/4$, the force is also anisotropic. The low-velocity heating for red detuning happens to be a general feature for $\phi\neq\pi/2$ as long as the saturation parameter s is sufficiently large. The fact that this heating effect only occurs at large laser intensity indicates that this behavior is related to the stimulated component of the force, also known as the dipole force.

In the left column of Fig. 4, we plot the corresponding steady-state momentum distribution calculated using the Monte Carlo wave function simulation method [17,18] for $2\beta=40\omega_r$. The momentum distributions are in full agreement with the semiclassical force plot shown in Fig. 3. In particular, one can see that for $\phi=\pi/2$, atoms accumulate around zero momentum, while for other values of ϕ, atoms will gather around some finite momenta corresponding to the critical points where the dipole heating force is balanced by the spontaneous cooling force.

To get a deeper understanding of the dipole force, the weak-field analytic approach is no longer valid. On the other hand, the dressed-state approach [19] usually provides a intuitive picture of the dipole force. For this purpose, we want

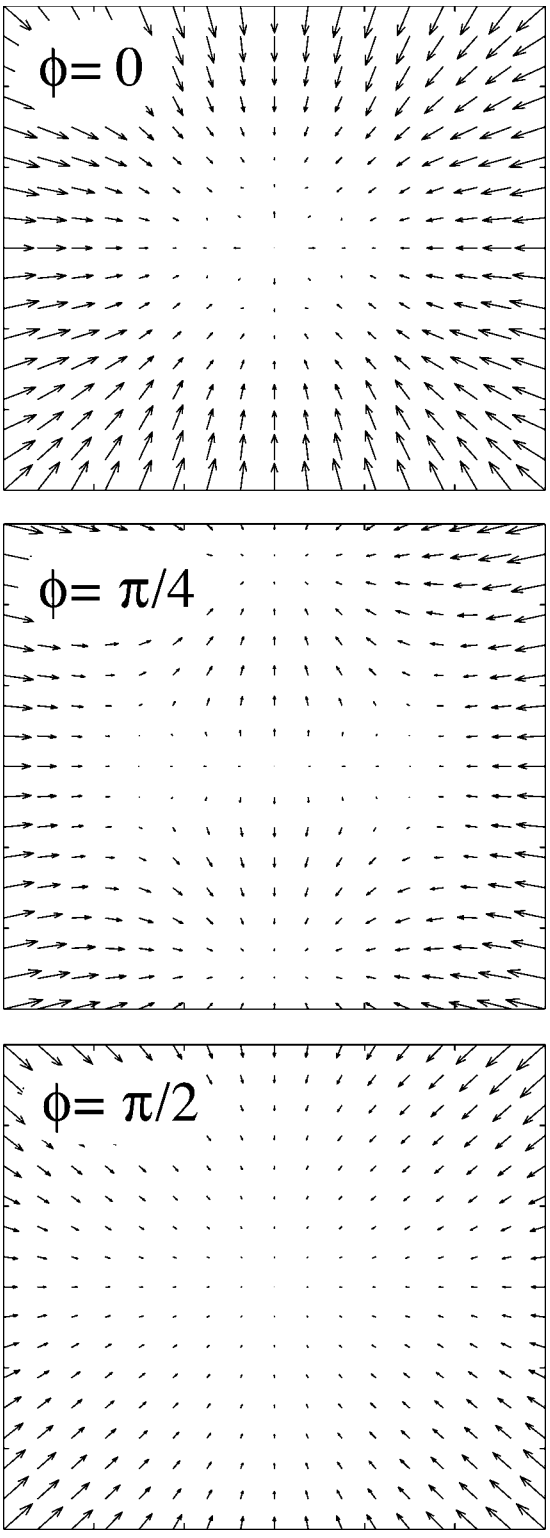

FIG. 3. Velocity-dependent force for $\Delta=-2\beta$ and $s=24.5$. The range of the velocity is $[-3,3]\beta/k$ along both axes.

to find the eigenvalues and eigenstates of the Hamiltonian (3).

The Hamiltonian (3) can be straightforwardly written in a 4×4 matrix form under the standard base states $(|g\rangle,|-\rangle,|0\rangle,|+\rangle)$. However, it turns out that we can change to a different base set $(|g\rangle,|e_1\rangle,|e_2\rangle,|e_3\rangle)$ through a unitary

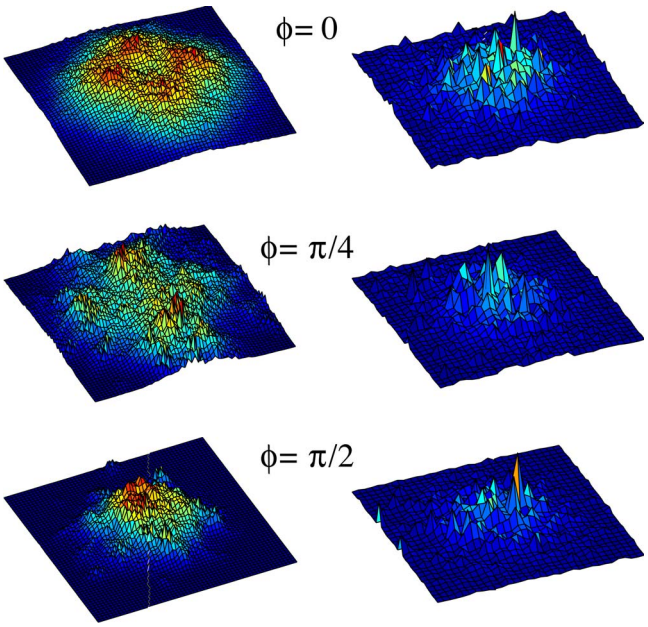

FIG. 4. (Color online). Steady-state momentum space distribution for $\Delta=-2\beta$ and $s=24.5$. Left column: broad-line transition with $2\beta=40\omega_r$. The range of the momentum is $[-30,30]\hbar k$, corresponding to a velocity range of $[-3,3]\beta/k$ along both axes; right column: narrow-line transition with $2\beta=1.6\omega_r$. The range of the momentum is $[-4,4]\hbar k$.

transformation over the excited-state manifold, where

$$|e_1\rangle=\frac{1}{\tilde{\Omega}}(\Omega_-^*|-\rangle+\Omega_0^*|0\rangle+\Omega_+^*|+\rangle),$$

$$|e_2\rangle=\frac{1}{\tilde{\Omega}\sqrt{|\Omega_+|^2+|\Omega_-|^2}}[\Omega_-^*\Omega_0|-\rangle+\Omega_+^*\Omega_0|+\rangle - (|\Omega_+|^2+|\Omega_-|^2)|0\rangle],$$

$$|e_3\rangle=\frac{1}{\sqrt{|\Omega_+|^2+|\Omega_-|^2}}(-\Omega_+|-\rangle+\Omega_-|+\rangle)$$

are linear superposition states of the original excited-state sublevels, with

$$\tilde{\Omega}^2=|\Omega_+|^2+|\Omega_0|^2+|\Omega_-|^2 = 2\Omega_x^2+2\Omega_y^2+4\cos\phi\Omega_x\Omega_y\cos kx\sin ky. \quad (8)$$

Under the transformed base set $(|g\rangle,|e_1\rangle,|e_2\rangle,|e_3\rangle)$, the Hamiltonian takes the block-diagonal form

$$H=\hbar\begin{pmatrix}0&\tilde{\Omega}/2&0&0\\ \tilde{\Omega}/2&-\Delta&0&0\\ 0&0&-\Delta&0\\ 0&0&0&-\Delta\end{pmatrix}, \quad (9)$$

from which we see that the states $|e_2\rangle$ and $|e_3\rangle$ are not coupled to the ground state $|g\rangle$ by the light field. These two states can be regarded as "dark states" that do not participate

in the atom-laser interaction and hence can be neglected. The remaining two states $|g\rangle$ and $|e_1\rangle$ form an effective two-level system that is dipole coupled with a coupling strength $\tilde{\Omega}$ given in Eq. (8).

The strong-field behavior of the light-pressure force can thus be easily understood from previous studies of a two-level atom interacting with standing light waves [15]. It is well known that in this case, under the strong-field and low-velocity limit, the Sisyphus effect gives rise to a heating force for red detuning and a cooling force for blue detuning [19], and the light-pressure force changes sign at some critical velocity. This therefore explains what we found numerically. The reason that no Sisyphus effect exists for $\phi=\pi/2$ can be seen from Eq. (8): when $\phi=\pi/2$, the effective coupling Ω becomes spatially independent; hence the standing-wave pattern responsible for the Sisyphus effect disappears. Obviously, when either Ω_x or Ω_y vanishes, $\tilde{\Omega}$ is again spatially independent, which provides an alternative way to understand the absence of the dipole force in a 1D σ^+-σ^- field.

We stress that the block-diagonal form of the Hamiltonian matrix given in Eq. (9) is *independent of the laser configuration*. Therefore, the reduction to the effective two-level atom is a generic feature of the $J_g=0\leftrightarrow J_e=1$ regardless of the dimensionality of the system. The Sisyphus effect should be present as long as the coupling constant $\tilde{\Omega}$ varies in space and its magnitude sufficiently large.

At blue detuning, the Sisyphus effect gives rise to a cooling dipole force which may have important applications. Whereas the spontaneous force saturates to a value of $\hbar k\beta$ at large laser intensity [see Eq. (4)], the stimulated force is not bounded by this limit. Figure 5 demonstrates the strong Sisyphus cooling force at blue detuing. Figure 5(a) shows the light-pressure force as a function of v_x at $v_y=0$. In comparison, the 1D force according to Eq. (4) is also plotted as the dashed line. At large velocity ($|v_x|\gtrsim 15\beta/k$), the 2D force is not very different from the 1D force, except that the former exhibits sharp resonance features that can be identified as Dopplerons [15,20] which arise from the coherent redistribution processes involving multiple photons. In contrast, the 2D force at small velocities is dominated by the Sisyphus effect: it becomes a cooling force within the velocity range $(-10,10)\beta/k$ and the maximum magnitude of the 2D force exceeds the 1D limit of $\hbar k\beta$. The force near zero velocity has a very steep slope, indicating a strong cooling capability.

At small velocities, the force can be expanded to first order in atomic velocity as

$$\mathbf{F}(\mathbf{v}) = -\eta\mathbf{v},$$

where η is the viscosity coefficient. For the 1D case, using Eq. (4), one can easily find that

$$\eta = -\frac{4s\Delta/\beta}{(1+s+\Delta^2/\beta^2)^2}\hbar k^2.$$

Hence $\eta>0$ (cooling force) when $\Delta<0$ and $\eta<0$ (heating force) when $\Delta>0$. Furthermore, η reaches the maximum value $\eta_{1D}=\hbar k^2/2$ under the optimal Doppler cooling condition $s=2$ and $\Delta=-\beta$. The 2D viscosity coefficient can be found numerically. Figure 5(b) displays η as a function of

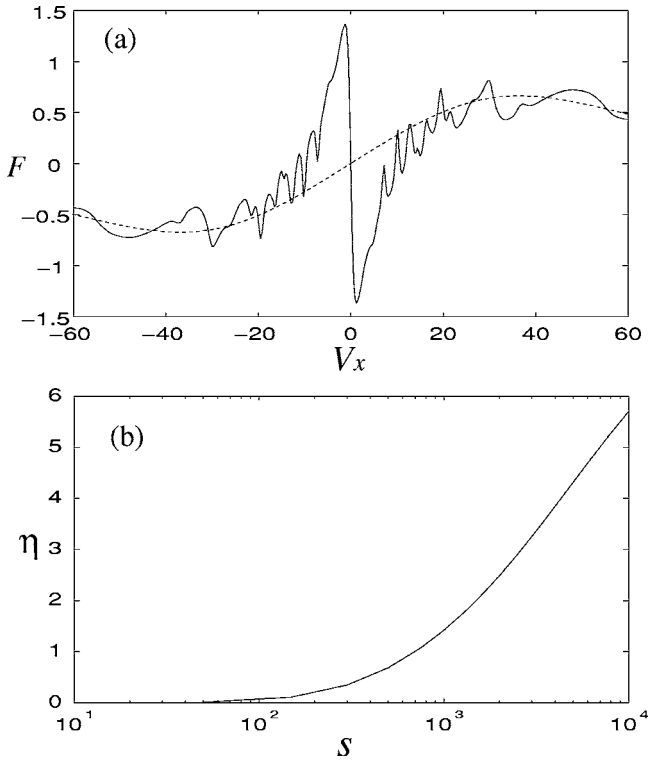

FIG. 5. (a) Velocity-dependent force for $\Delta=30\beta$, $s=2000$, $\phi=0$, and $v_y=0$. Solid line: 2D force. Dashed line: 1D force according to Eq. (4). The velocity is in units of β/k and the force in units of $\hbar k\beta$. (b) The viscosity coefficient η (in units of $\hbar k^2$) as a function of the saturation parameter s.

the saturation parameter s for the 2D force with a blue detuning. For this set of parameters, η becomes positive when $s\geqslant 26$. At large s, the 2D viscosity coefficient can exceed η_{1D} by over an order of magnitude. We note that 1D Sisyphus cooling with blue-detuned laser light has been observed in experiments [21].

Even though the Sisyphus effect is capable of producing very strong cooling forces, it however does not lead to a lower temperature at equilibrium compared with the normal spontaneous force-based red-detuned low-intensity optical molasses. This is because the induced momentum diffusion coefficient D scales roughly as the saturation parameter s at large laser intensity, while the viscosity coefficient for the dipole cooling force $\eta\sim\sqrt{s}$ under the same limit [19,22]. The temperature at equilibrium $T\sim D/\eta\sim\sqrt{s}$ thus increases as laser intensity increases. Therefore, for a broad-line $0\leftrightarrow 1$ transition, the blue Sisyphus cooling force is *not* capable of producing temperatures below the Doppler limit.

IV. RESULTS FOR NARROW-LINE TRANSITION

Narrow-line transitions correspond to atomic transitions where the excited-state spontaneous emission rate is comparable to or even smaller than the single-photon recoil frequency. Theoretical study of Doppler cooling on a narrow-line $0\leftrightarrow 1$ transition under the 1D σ^+-σ^- field configuration has shown that subrecoil temperature can be reached [23], as

was demonstrated in recent experiments [13]. The semiclassical treatment we used above to describe the broad-line cooling relies on a perturbative expansion of $mv/(\hbar k)$ and is therefore not suitable for narrow-line studies where the atomic momentum can become comparable to the single-photon recoil momentum. To study the cooling properties in the narrow-line regime, one must use a full quantum-mechanical treatment in which the atomic center-of-mass motion is also quantized.

For the 1D σ^+-σ^- laser field, the problem is greatly simplified due to the lack of a coherent photon redistribution. A density-matrix master equation approach can be adopted [23]. The situation becomes significantly more complicated at higher dimensions as now a coherent photon redistribution becomes possible. We use the Monte Carlo method to find the steady-state momentum distribution for the 2D field configuration, and the result is displayed in the right column of Fig. 4.

For our calculation, we choose $2\beta=1.6\omega_r$ which corresponds to the narrow-line $^1S_0$-$^3P_1$ intercombination transition of ^{88}Sr. Comparing the two columns in Fig. 4, we see two important differences between the broad- and narrow-line transitions: (1) the momentum distribution for the narrow-line transition is not as sensitive to the phase ϕ as for the broad-line transition, and (2) there is no apparent Sisyphus effect in the narrow-line transition as the atoms accumulated around zero momentum for all values of ϕ. The differences might be understood as follows: Changing the phase ϕ would change the laser field distribution over a length scale on the order of laser wavelength λ. For narrow-line cooling, temperatures about the single-photon recoil are reached. Hence the atomic de Broglie wavelength, which can be regarded as the effective size of the atom, is comparable to the laser wavelength. The atom therefore experiences an effective laser field averaged over its de Broglie wavelength. This averaging reduces the sensitivity to the phase ϕ and also explains the lack of Sisyphus effect which relies on the presence of the light shift spatially modulated with a period of $\lambda/2$ [19].

A closer examination of the narrow-line momentum distribution does show some weak ϕ dependence; namely, the width of the distribution decreases slightly when ϕ changes from 0 to $\pi/2$. This can be attributed to the standing-wave pattern present in the 2D field configuration which causes atomic diffraction and hence broadens the momentum distribution.

The JILA experiment reported in Ref. [13] concerns the narrow-line cooling on the $^1S_0$-$^3P_1$ transition of ^{88}Sr. One particular set of experiments is carried out in a 3D optical molasses with blue laser detuning. They found that the atoms organize into discrete momentum packets forming a face-centered-cubic crystal, a behavior which can be rather satisfactorily explained by the 1D force equation given in Eq. (4). This is in accordance with our calculation here which shows that narrow-line transitions do not exhibit strong multidimensional effects.

V. CONCLUSION

In conclusion, we have performed a detailed study of the $J_g=0\leftrightarrow J_e=1$ transition under a 2D σ^+-σ^- laser field. Our work shows that inherent multidimensional effects are expected in broad-line transitions. These multidimensional effects are in general sensitive to the time-phase difference ϕ between fields along different dimensions. In most experimental situations, ϕ is not deliberately stabilized. When ϕ fluctuates randomly, the multidimensional effects are washed out and become unobservable. It is therefore crucial to stabilize ϕ, as was done in the experiment reported in Ref. [6], in order to observe the multidimensional cooling effects. Otherwise, the multidimensional light-pressure force may indeed be regarded as a simple superposition of 1D forces. This shows why the 1D cooling theories are as successful as they are in explaining 2D and 3D experimental results.

Our work also shows that qualitative differences exist between the broad- and narrow-line transitions. In particular, narrow-line transitions do not exhibit strong multidimensional effects or Sisyphus effects.

One interesting point we have found in this calculation is that, due to the presence of the two dark states which are linear superpositions of the excited sublevels, the broad-line $J_g=0\leftrightarrow J_e=1$ transition can be reduced to an effective two-level atom regardless of the laser configuration. Therefore there exists a Sisyphus cooling force at blue laser detuning as long as the laser fields support a standing-wave pattern. Because of the stimulated nature of the Sisyphus effect, this cooling force does not saturate at large laser intensity and, hence, can be significantly more efficient than the spontaneous cooling force of the 1D Doppler theory. This, however, does not lead to sub-Doppler temperatures at equilibrium since a large laser intensity also results in large momentum diffusion. From a theoretical point of view, this reduction to an effective two-level structure may simplify future theoretical studies of the $J_g=0\leftrightarrow J_e=1$ transition.

By contrast, for a narrow-line transition, due to the lack of the Sisyphus effect, we cannot take advantage of the large cooling capability of the dipole force. Temperatures comparable to the sing-photon recoil limit have been achieved using Doppler cooling on narrow-line transitions. This, by its own, is not yet enough to reach quantum degeneracy [24]. How to further improve the narrow-line cooling efficiency and whether one can achieve all-optical quantum degeneracy without the time-consuming evaporative cooling process are still open questions and remain as both theoretical and experimental challenges.

ACKNOWLEDGMENTS

We thank Professor Tom Killian for valuable discussions. This work is supported by Rice University and partially supported by the REU program sponsored by the National Science Foundation under Grant No. 0139202.

APPENDIX A: ANALYTIC EXPRESSIONS OF THE VELOCITY-DEPENDENT FORCE FOR THE BROAD-LINE TRANSITION

In this appendix, we outline the details of how the analytic expressions of the velocity-dependent force can be obtained following Ref. [16].

First we write down the optical Bloch equations—i.e., the equations of motion for ρ_{ij}. We will work in the weak-field limit by assuming that $\Omega_{\pm,0}^2/(\beta^2+\Delta^2) \ll 1$. We will neglect any terms that are of the second or higher orders of this small quantity. Under this limit, the excited-state coherences (e.g., ρ_{23}, ρ_{24}, ρ_{34} and their respective conjugates) vanish. The remaining equations are

$$\dot{\rho}_{\alpha\alpha} = -2\beta\rho_{\alpha\alpha} + i\frac{\Omega_\alpha}{2}\rho_{\alpha g} - i\frac{\Omega_\alpha^*}{2}\rho_{g\alpha}, \tag{A1a}$$

$$\dot{\rho}_{g\alpha} = (-\beta + i\Delta_\alpha)\rho_{g\alpha} - i\frac{\Omega_\alpha}{2}(\rho_{gg} - \rho_{\alpha\alpha}), \tag{A1b}$$

where $\alpha = -, 0, +$ and we need to add the population conservation condition

$$\rho_{gg} = 1 - \rho_{--} - \rho_{00} - \rho_{++}.$$

Here we have included the effect of a magnetic field along the quantization axis by defining

$$\Delta_\pm = \Delta \mp \omega_B, \quad \Delta_0 = \Delta.$$

The zero-velocity steady-state solution can be easily obtained by taking the time derivatives to be zero, which yields

$$\rho_{\alpha\alpha}^{(0)} = \Sigma_\alpha = \frac{|\Omega_\alpha|^2}{4(\beta^2 + \Delta_\alpha^2)} \quad (\alpha = -, 0, +),$$

$$\rho_{g\alpha}^{(0)} = i\frac{\Omega_-}{2(\beta - i\Delta_+)}(\rho_{gg}^{(0)} - \rho_{\alpha\alpha}^{(0)}).$$

We now find the solution, to first order in velocity, by taking the time derivatives on the left-hand side of Eqs. (A1) as

$$\dot{\rho}_{ij} = \mathbf{v} \cdot \boldsymbol{\nabla} \rho_{ij}^{(0)},$$

and resolve the optical Bloch equations. This procedure yields the first-order solution as

$$\rho_{\alpha\alpha}^{(1)} = \Sigma_\alpha - \frac{1}{2\beta}\mathbf{v} \cdot \boldsymbol{\nabla}\Sigma_\alpha,$$

$$\rho_{g\alpha}^{(1)} = \frac{1}{\beta - i\Delta_\alpha}\left[i\frac{\Omega_\alpha}{2}(\rho_{gg}^{(1)} - \rho_{\alpha\alpha}^{(1)}) - \mathbf{v} \cdot \boldsymbol{\nabla}\rho_{g\alpha}^{(0)} \right].$$

The velocity-dependent force can then be found as

$$\mathbf{F}(\mathbf{v}) = -\overline{\langle \boldsymbol{\nabla} H \rangle} = \hbar\, \mathrm{Re}\left[\sum_{\alpha=-,0,+} \overline{\rho_{g\alpha}^{(1)} \boldsymbol{\nabla} \Omega_\alpha^*} \right],$$

where the overbar represents average over one optical wavelength along both the x and y directions.

APPENDIX B: EFFECTS OF MAGNETIC FIELD

We have so far neglected any external magnetic field. Under many circumstances, a magnetic field is present. This occurs, for example, during the operation of a MOT. Here we consider the simplified case where a uniform field with strength B is applied along the quantization axis, in order to illustrate the new features induced by the magnetic field.

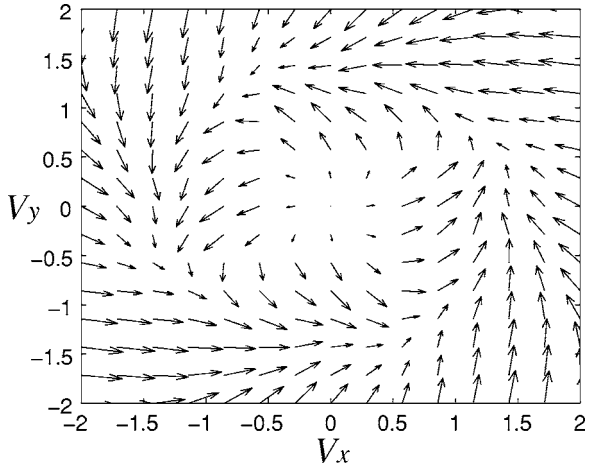

FIG. 6. Velocity-dependent force for $\Delta = -\beta$, $\omega_B = 4\beta$, $\phi = \pi/2$, and $s = 100$. The velocity is in units of β/k.

The Zeeman effect due to this field will lift the energy degeneracy of the excited manifold, assuming the field is not too strong so that the quadratic Zeeman effect can be neglected. While the states $|0\rangle$ and $|g\rangle$ are not affected by the external field, the states $|\pm\rangle$ will be shifted by the amount $\pm\hbar\omega_B = \pm\gamma B$, respectively, with γ being the gyromagnetic ratio. We performed numerical calculations under such a condition for the case of the broad-line transition and found that the features in the absence of the magnetic field are preserved. In particular, the Sisyphus effect can still be observed. This is despite the fact that we can no longer reduce the system to an effective two-level atom as there are no dark states when the excited state degeneracy is lifted.

One new feature induced by the magnetic field is the "vortical force" as shown in Fig. 6, which illustrates a strong-field situation where both the vortical force and the Sisyphus effect can be clearly seen.

Analytical expressions for the vortical force can again be found in the weak-field low-velocity limit. The vortical force can be written as

$$\mathbf{F}_{\mathrm{vor}}(\mathbf{v}) = \alpha_{\mathrm{vor}}\hbar k^2(v_y\hat{x} - v_x\hat{y}),$$

with the coefficient

$$\alpha_{\mathrm{vor}} = \frac{\beta^2\Omega^2}{16(\beta^2+\Delta^2)}\left[\frac{1}{(\Delta+\omega_B)^2+\beta^2} - \frac{1}{(\Delta-\omega_B)^2+\beta^2} \right]\cos 2\phi \simeq \frac{\beta^2\Delta\Omega^2\omega_B}{16(\Delta^2+\beta^2)^3}\cos 2\phi,$$

where the last line is valid for a weak magnetic field when $\omega_B^2 \ll \beta^2 + \Delta^2$. Therefore the vortical force is analogous to the Lorentz force experienced by a charged particle moving in a magnetic field. The effective charge would be

$$Q_{\text{eff}} = \frac{\beta^2 \Delta\Omega^2 \gamma k^2}{16(\Delta^2 + \beta^2)^3} \cos 2\phi.$$

For the parameters of Fig. 6, this yields $Q_{\text{eff}} = 5.7 \times 10^{-18}$ C, or about 35 electron charge, for the $5\,{}^1S_0 - 5\,{}^1P_1$ broad-line transition of ^{88}Sr.

The other new force induced by the magnetic field can be written as

$$\mathbf{F}'_{\text{ani}}(\mathbf{v}) = \alpha'_{\text{ani}} \hbar k^2 (v_y \hat{x} + v_x \hat{y}),$$

which represents an anisotropic force along the two diagonal directions $\hat{x}+\hat{y}$ and $\hat{x}-\hat{y}$. This force varies as $\sin 2\phi$, but is usually rather weak and hence is dominated by other types of forces.

Obviously, the magnetic field used in the MOT is not uniform. To realistically model the force inside a MOT, we have to account for the spatial variance of the magnetic field in both magnitude and direction. This is a rather complicated situation, out of the scope of this paper. Again, a Monte Carlo approach seems to be the only possible way to tackle this problem. Nevertheless, our calculations indicate that the magnetic-field-induced multidimensional features may play a nontrivial role in the dynamics of a MOT.

Finally, we also studied the effects of the magnetic field on the narrow-line transition. No appearance of the vortical force is found in this case. In general, the magnetic field does not seem to play as a significant role in the narrow-line transition as in the broad-line transition.

[1] H. J. Metcalf and P. van der Straten, *Laser Cooling and Trapping* (Springer, New York, 1999).

[2] A. P. Kazantsev and I. V. Krasnov, J. Opt. Soc. Am. B **6**, 2140 (1989).

[3] K. Mølmer, K. Berg-Sorensen, and E. Bonderup, J. Phys. B **24**, 2327 (1991).

[4] T. Cai and N. P. Bigelow, Opt. Lett. **19**, 1768 (1994).

[5] H. Pu, T. Cai, and N. P. Bigelow, Eur. Phys. J. D **7**, 269 (1999); N. P. Bigelow *et al.*, Acta Phys. Pol. A **86**, 29 (1994).

[6] A. Hemmerich, D. Schropp, and T. W. Hänsch, Phys. Rev. A **44**, 1910 (1991); A. Hemmerich and T. W. Hänsch, Phys. Rev. Lett. **68**, 1492 (1992).

[7] E. L. Raab *et al.*, Phys. Rev. Lett. **59**, 2631 (1987).

[8] T. Binnewies *et al.*, Phys. Rev. Lett. **87**, 123002 (2001); J. Grünert and A. Hemmerich, Phys. Rev. A **65**, 041401(R) (2002); E. A. Curtis, C. W. Oates, and L. Hollberg, J. Opt. Soc. Am. B **20**, 977 (2003).

[9] H. Katori, T. Ido, Y. Isoya, and M. Kuwata-Gonokami, Phys. Rev. Lett. **82**, 1116 (1999); T. Ido, Y. Isoya, and J. Katori, Phys. Rev. A **61**, 061403(R) (2000).

[10] T. Loftus, J. R. Bochinski, and T. W. Mossberg, Phys. Rev. A **66**, 013411 (2002).

[11] S. B. Nagel *et al.*, Phys. Rev. A **67**, 011401(R) (2003).

[12] T. P. Dinneen *et al.*, Phys. Rev. A **59**, 1216 (1999); G. Zinner *et al.*, Phys. Rev. Lett. **85**, 2292 (2000); M. Machholm, P. S. Julienne, and K. A. Suominen, Phys. Rev. A **64**, 033425 (2001); T. Ido *et al.*, Phys. Rev. Lett. **94**, 153001 (2005).

[13] T. H. Loftus *et al.*, Phys. Rev. Lett. **93**, 073003 (2004); T. H. Loftus *et al.*, Phys. Rev. A **70**, 063413 (2004);

[14] Phys. Rev. A **60**, R745 (1999); Y. Takasu *et al.*, Phys. Rev. Lett. **91**, 040404 (2003).

[15] V. S. Letokhov and V. G. Minogin, Phys. Rep. **73**, 1 (1981); S. Stenholm, Rev. Mod. Phys. **58**, 699 (1986).

[16] J. P. Gordon and A. Ashkin, Phys. Rev. A **21**, 1606 (1980).

[17] J. Dalibard, Y. Castin, and K. Mølmer, Phys. Rev. Lett. **68**, 580 (1992); K. Mølmer, Y. Castin, and J. Dalibard, J. Opt. Soc. Am. B **10**, 524 (1993).

[18] H. Carmichael, *An Open Systems Approach to Quantum Optics* (Springer, Berlin, 1993).

[19] J. Dalibard and C. Cohen-Tannoudji, J. Opt. Soc. Am. B **2**, 1707 (1985).

[20] H. Pu, T. Cai, and N. P. Bigelow, Laser Phys. **4**, 969 (1994).

[21] R. Gupta *et al.*, Phys. Rev. Lett. **71**, 3087 (1993); C. A. Sackett, C. C. Bradley, and R. G. Hulet, Laser Phys. **4**, 861 (1994).

[22] A. V. Bezverbnyi *et al.*, JETP **96**, 383 (2003).

[23] Y. Castin, H. Wallis, and J. Dalibard, J. Opt. Soc. Am. B **6**, 2046 (1989); H. Wallis and W. Ertmer, *ibid.* **6**, 2211 (1989).

[24] Using a conventional MOT operating on the narrow-line transition of ^{88}Sr, a phase-space density of 10^{-2}, which is 3 orders of magnitude larger than that in broad-line MOT, has been achieved as reported in the experiment of Ref. [9].